SIMULTANEOUS NEUTRON AND X-RAY IMAGING OF 3D KEROGEN AND FRACTURE STRUCTURE IN SHALES

Wei-Shan Chiang[†,‡,⊥], Jacob M. LaManna[¶], Daniel S. Hussey[¶], David L. Jacobson[¶], Yun Liu[‡,⊥,#], Jilin Zhang[†], Daniel T. Georgi[†], and Jin-Hong Chen[†]

[†]Reservoir Engineering Technology, Aramco Research Center – Houston

[‡] Center for Neutron Research, National Institute of Standards and Technology, Gaithersburg, Maryland

[⊥] Department of Chemical and Biomolecular Engineering, University of Delaware, Newark, Delaware, USA

[¶]Physical Measurement Laboratory, National Institute of Standards and Technology, Gaithersburg, Maryland

[#]Department of Physics and Astronomy, University of Delaware, Newark, Delaware, USA

This paper was prepared for presentation at the SPWLA 58th Annual Logging Symposium held in Oklahoma City, Oklahoma, USA, June 17-21, 2017.

ABSTRACT

Hydrocarbon production from shales using horizontal drilling and hydraulic fracturing has been the key development in the US energy industry in the past decade and has now become more important globally. Nevertheless, many fundamental problems related to the storage and flow of light hydrocarbons in shales are still unknown. It has been reported that the hydrocarbons in the shale rocks are predominantly stored within the kerogen pores with characteristic length scale between 1 nm to 100 nm. In addition, the 3D connectivity of these kerogen pores and fractures from the micrometer to centimeter scale form the flow path for light hydrocarbons. Therefore, to better model the gas-in-place and permeability in shales, it is necessary to quantify the structural distribution of organic and inorganic components and fractures over a large breadth of length scales.

Simultaneous neutron and X-ray tomography offers a core-scale non-destructive method that can distinguish the organic matter, inorganic minerals, and open and healed fractures in 2.5 cm diameter shales with resolution of about 30 μm and field of view of about 3 cm. In the reconstructed neutron volume, the hydrogen-rich areas, i.e. organic matter, are brighter because hydrogen has a larger attenuation coefficient and attenuates neutron intensity more significantly. For the X-ray volume, the attenuation coefficient of an element is related to its atomic number Z and the brighter areas indicate the region containing more high-Z elements such as minerals. Open fractures do not attenuate either neutrons or X-rays and therefore look dark in both reconstructed neutron and X-ray volumes.

In this study, two shale samples from different locations were investigated using simultaneous neutron and X-ray tomography for the first time. We were able to construct 3D images of shales and isolate 3D maps of organic matter and high-Z minerals. The distribution of kerogen and fractures can be used in the modeling of hydrocarbon flow in core scale, a 10^9 upscaling from current methods that model the flow based on SEM images.

Q

INTRODUCTION

Natural gas production worldwide from shale resources is projected to grow from 1.2×10^9 m^3/d in 2015 to 4.8×10^9 m^3/d by 2040 (Aloulou and Zaretskaya 2016). Shale gas is predicted to account for 30% of world natural gas production by 2040 (Aloulou and Zaretskaya 2016). Despite the promising future of shale gas as an energy source, fundamental problems related to the storage and transport of hydrocarbons in shales still lack clear understanding. The organic matter in organic rich source rocks may include kerogen, bitumen, and/or heavier immobile hydrocarbons. Kerogen is imbedded within the inorganic matrix of shale rocks and does not dissolve in any solvent (Loucks et al. 2009). Previous studies have suggested that the majority of light hydrocarbons in the shale rocks are stored within the kerogen which has pores with the characteristic length scale between 1 to 100 nm (Ambrose et al. 2013). The total amount and the distribution of kerogens in the shales, therefore, can influence the total gas in place (GIP) of the shales. Moreover, the kerogens and minerals in shales have very

different properties such as pore structure (pore size, pore shape, and pore connectivity), surface chemistry, wettability, and mechanical response. These properties are directly related to the interaction of hydrocarbons with pore surfaces. Thus, the structure and three-dimensional (3D) space arrangement of the components within the rocks can significantly influence the flow path of the hydrocarbons in the shales. To better understand the storage and transport properties of hydrocarbons within the shale rocks, it is necessary to identify the distribution and the structure of organic components, especially the kerogens, and inorganic components, i.e. the minerals, and fractures in the rocks.

The development of focused ion beam-scanning electron microscopy (FIB-SEM) enables the visualization of the localized pores, kerogens, and inorganic matrix in small shale samples (Loucks et al. 2009). Moreover, the FIB-SEM images have been used to construct the 3D pore scale representations as the input to the simulation and modeling of hydrocarbon transport in the shales (Jiang et al. 2017; Shabro et al. 2013). However, the structure of the rocks and flow properties obtained from FIB-SEM are at the pore scale. There is also the need to obtain the distribution of organic matter, kerogen and fractures at the core scale.

In the petroleum industry, X-ray computed tomography (CT) is a common tool to characterize the structure of source rocks. X-rays interact with electrons of the materials and, therefore, the attenuation coefficient of X-ray is proportional to the atomic number, Z, of the elements in the materials. High-Z elements such as metals can significantly attenuate X-rays and produce high contrast in the X-ray CT image. This makes X-ray CT a powerful tool to identify the mineral distribution inside the samples. However, organic matter, which is ubiquitous in natural materials, is mainly composed of low-Z elements such as hydrogen and carbon. These materials only have small interaction with X-rays and are fairly transparent to X-rays. What is more, when fractures and pores are present in the samples, it is hard for X-rays to distinguish between these "empty" spaces and the organic matter.

Unlike X-rays, neutrons interact with the atomic nuclei of elements inside the materials. The attenuation coefficient for neutrons has little correlation with Z (Banhart et al. 2010). In particular, hydrogen, which is the most transparent element for X-ray and is very abundant in organic matter, has a very large attenuation coefficient for neutron. The high sensitivity of neutron to organic matter makes neutron imaging a complementary tool to the widely-used X-ray CT for thoroughly and correctly characterizing the structure and components of the heterogeneous shale samples at the core scale. Dual neutron and X-ray tomography has been successfully applied to many other materials such as fuel cells (Banhart et al. 2010; Manke et al. 2007b), batteries (Manke et al. 2007a), and cultural heritage objects (Mannes et al. 2015; Mannes et al. 2014).

In this study, for the first time, "simultaneous" dual X-ray and neutron imaging is used to study shales at the core scale at the National Institute of Standards and Technology (NIST) Center for Neutron Research (NCNR). The distributions of minerals, organic matter and fractures are successfully identified in a Barnett shale and a Middle East shale. The distribution of organic matter is found to have very different configuration and distribution in these two shales.

METHOD

Attenuation of X-ray and neutron by materials. X-ray imaging and neutron tomography are both non-invasive methods and have similar principles. When an incident X-ray or neutron beam with intensity I_0 interacts with a material, the X-ray or neutron intensity is attenuated by different interaction processes. For a homogeneous medium with thickness d, the transmitted intensity of X-rays or neutrons can be described by the Lambert-Beer law:

$$I_t = I_0 \, e^{-\mu \cdot d} \qquad (1)$$

μ is the attenuation coefficient, which is a material property and depends on the incident radiation, i.e. X-ray or neutron, and incident radiation energy. μ can be related to atomic composition of the material by

$$\mu = \sum_i \sigma_{t,i} \, N_i \qquad (2)$$

$\sigma_{t,i}$ is the total attenuation cross section for X-ray or neutron and N_i is the number density of type i

atom. μ is very different for X-rays and for neutrons because the X-rays interact with electrons while neutrons interact with nuclei in the materials.

For X-rays, the intensity attenuation is due to Thomson (coherent) scattering, photoelectric absorption, Compton scattering, and pair production. Thus, the total cross section for X-rays for atom *i*, $\sigma_{i,t}^{X-ray}$, can be written as

$$\sigma_{i,t}^{X-ray} = \sigma_i^{TS} + \sigma_i^{PA} + \sigma_i^{CS} + \sigma_i^{PP} \qquad (3)$$

σ_i^{TS}, σ_i^{PA}, σ_i^{CS}, and σ_i^{PP} are X-ray atomic cross sections for Thomson scattering, photoelectric absorption, Compton scattering, and pair production, respectively. Pair production is ignored because the peak energy of 90 keV of the X-ray tube used in this work is well below the 1.022 MeV threshold for its occurrence.

Neutron has many ways to interact with matter characteristic of different cross sections such as elastic scattering (σ_i^{ES}), inelastic scattering (σ_i^{IES}), radiative capture (σ_i^{RC}), and fission (σ_i^{F}). Thus, the total cross section for neutron for atom *i*, $\sigma_{i,t}^{Neutron}$, can be written as

$$\sigma_{i,t}^{Neutron} = \sigma_i^{ES} + \sigma_i^{IES} + \sigma_i^{RC} + \sigma_i^{F} + \cdots \quad (4)$$

For heterogeneous materials, the integral form should be used:

$$I_t = I_0\, e^{-\int_l \mu(x)dx} \qquad (5)$$

l denotes the transmission path and *x* is a 3-dimensional position vector. The transmission of the beam through the sample depends upon the map of the attenuation coefficient μ (*x*) and transmission path.

Table 1 lists the attenuation coefficient, μ, for several common elements found in shales for X-ray and neutron at relevant conditions. Attenuation coefficients for neutron and X-ray are calculated by using Neutron Activation and Scattering Calculator provided by NCNR (Kienzle) and X-Ray Form Factor, Attenuation, and Scattering Tables provided by NIST Physical Measurement Laboratory (Seltzer), respectively. Clearly, hydrogen containing materials have large attenuation coefficient for neutrons compared with hydrogen-free elements.

Table 1. The attenuation coefficient of X-ray and neutron for common elements in shales

Component	μ for X-ray 90 keV[a] (cm^2/g)	μ for neutron 1.8 Å[b] (cm^2/g)
Kerogen[c] ($C_{100}H_{161}N_{1.85}S_{0.7}O_{9.2}$)	0.22	6.97
Quartz (SiO_2)	0.48	0.29
Pyrite (FeS_2)	1.66	0.44
Siderite ($FeCO_3$)	1.20	0.67
Calcite ($CaCO_3$)	0.58	0.35
Dolomite ($CaMg(CO_3)_2$)	0.55	0.41
Fluorapatite $Ca_5(PO_4)_3F$	0.71	0.31
Anhydrite ($CaSO_4$)	0.64	0.29
Kaolinite ($Al_2Si_2O_5(OH)_4$)	0.47	2.32
Chlorite ($Mg_5Al_2Si_3O_{10}(OH)_8$)	0.44	2.07
Daphnite ($Fe_5Al_2Si_3O_{10}(OH)_8$)	0.95	2.30
H_2O	0.18	5.65
C_6H_{14}	0.12	5.39

[a]90 keV is the peak X-ray energy for the spectrum generated by the X-ray tube in this measurement. Attenuation coefficient for X-ray is obtained from X-Ray Form Factor, Attenuation, and Scattering Tables (Seltzer).

[b]The neutrons used in this study are thermal neutrons with a Maxwell-Boltzmann distribution centered around 1.8 Å wavelength. Attenuation coefficient for neutron is obtained from Neutron Activation and Scattering Calculator (Kienzle).

[c]Formula obtained from literature (Siskin et al. 1995).

Samples. Two samples were used in this study. The first one, provided by Bureau of Economic Geology (BEG), is a Barnett shale from T.P. Sims #2 well in the Fort Worth Basin. The characterization of this sample can be found in previous study (Louck et all 2009; Zhang et al. 2014). It has Vitrinite Reflectance *Ro* = 1.61 % and total organic carbon (TOC) = 3.64 %. A

second sample is an organic-rich carbonate source rock from the Middle East and shall be named Middle East shale. The samples are 2.5 cm in diameter and approximately 2 cm in length.

Experimental set-up. Experiments were conducted at NCNR on the BT2 neutron imaging facility. This instrument offers a high thermal neutron flux for radiography and tomography. A 90 keV microfocus X-ray generator is located perpendicular to the neutron beam at the sample location to allow simultaneous neutron and X-ray tomography. Full details of the instrument can be found in the following manuscript (LaManna et al. 2017). Detector resolution was set to 30 µm for both neutron and X-ray detectors to keep the sample in the field-of-view at all projection angles. Each scan took approximately 18 hours to complete. Volumes were reconstructed from the projection images using the commercial CT software package Octopus[1] and visualized with the open-source Drishti Volume Exploration Tool (Limaye 2012).

RESULTS

The two shales were studied using the simultaneous X-ray and neutron tomography to extract the 3D structure and spatial arrangement of their components such as minerals, organic matter, and fractures in the rocks.

Barnett shale. Figure 1 shows the simultaneous X-ray and neutron CT reconstruction slices for the Barnett shale. The brighter parts of the image indicate regions with larger attenuation, while the darker parts correspond to regions with less attenuation. For neutrons, the hydrogen-rich areas are brighter because hydrogen has larger cross section and attenuates neutron intensity more significantly. For X-rays, the cross section of an element is proportional to its atomic number Z and the brighter areas indicate the regions containing more high-Z elements such as heavy minerals.

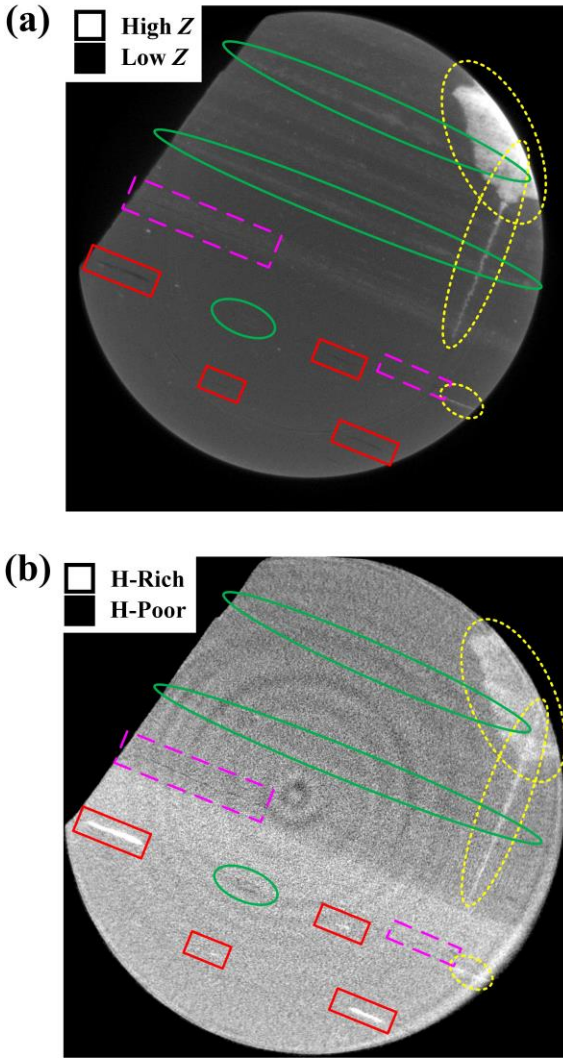

Fig. 1 Upper slices of (a) X-ray and (b) neutron reconstructed volumes of the Barnett shale sample. The short-dashed yellow ovals and solid green ovals outline the mineral components of pyrite and apatite, respectively. Solid red rectangles outline the organic-rich regions likely to be kerogens, the long-dashed magenta rectangles outline the open fractures.

Layered patterns are apparent in the upper part of the sample in both X-ray and neutron tomography slices (Figure 1). The bright layers in the X-ray slice indicate that these layers have high atomic number and, therefore, are composed of minerals (see the layers outlined by the solid green ovals). These bright layers in X-ray slice correspond to

[1] Certain trade names and company products are mentioned in the text or identified in an illustration in order to adequately specify the experimental procedure and equipment used. In no case does such identification imply recommendation or endorsement by the National Institute of Standards and Technology, nor does it imply that the products are necessarily the best available for the purpose.

the dark layers in neutron slice. There is also a bright pocket connected with a bright sharp line on the upper right of the slice for both neutron and X-ray images (outlined by short-dashed yellow ovals). This indicates that element in this region has high atomic number and at the same time can strongly attenuate neutron intensity. This area can possibly be occupied by minerals with high mass density iron-rich components which exist in common shale minerals. It should be noticed that the bright layers and bright pocket shown in X-ray slice are composed of different minerals. These two minerals can be easily distinguished in the neutron slice where the layers look dark while the pocket looks bright. The large bright pocket in both X-ray and neutron images is pyrite. The stripes bright in X-ray but dark in neutron are Fluorapatite (see Table 1 for attenuation coefficients and Appendix for XRD result).

Neutron image shows sporadic bright stripes which correspond to the dark stripes in the X-ray image as outlined by the solid red rectangles in Figure 1. The stripes are regions with concentrated hydrogen which attenuate neutrons but are transparent to X-rays. The hydrogen-rich areas are quite likely to be organic kerogen. There are also regions that look dark in both neutron and X-ray images in Figure 1 (outlined by the long-dashed magenta rectangles). Because the "element" is transparent to and therefore has no interaction with both neutron and X-ray, it is reasonable to identify the lines within the long-dashed magenta rectangles in Figure 1 as fractures. If X-ray is the only imaging source (Figure 1(a)), it is hard to distinguish between the organic matter (solid red rectangles) and the fractures (long-dashed magenta rectangles). With the aid of neutron imaging, the two different components can be easily recognized.

The lower part of the neutron slice is homogenously brighter than upper part, indicating that the hydrogen content is higher in the lower part rather than in the upper part of the sample. This is consistent with the fact that the upper part is composed of the layered and pocket inorganic matter containing minerals.

Figure 2(a) and 2(b) are the 3D X-ray and neutron volume renderings of the T.P. Sims #2 well sample, respectively. The colored regions show the highly attenuated areas. The rock sample can be divided into two parts: one with the mineral-rich region containing layers of Fluorapatite and a pocket connecting to a healed fracture filled with

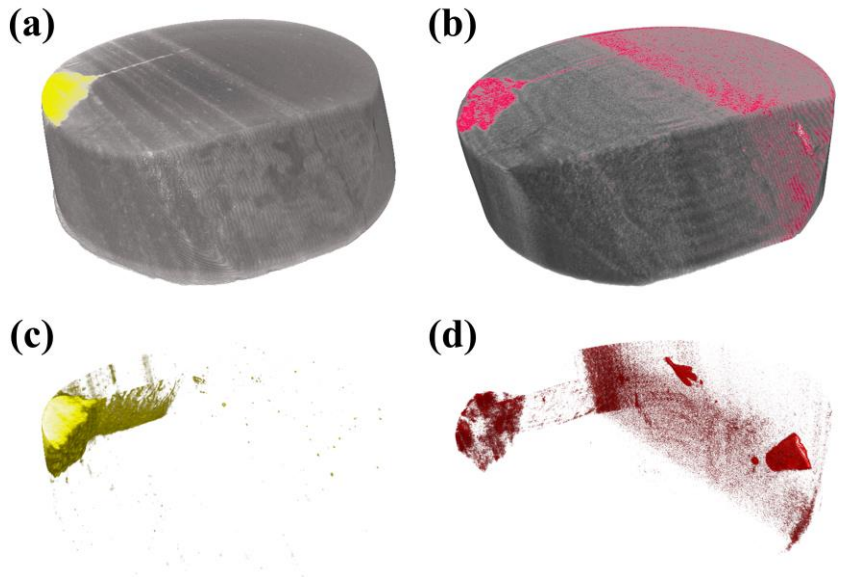

Fig. 2 3D volume renderings of the Barnett shale sample for (a) X-ray and (b) neutron tomography. Distributions of (c) high-Z components, i.e. the minerals, showing a pyrite pocket and a healed fracture; and (d) hydrogen-rich components, likely to be kerogens, are identified by isolating the appropriate peak in the grayscale histograms.

pyrite; the other with a relatively homogeneous hydrogen-rich region similar to that seen in the slices shown in Figure 1. By setting a high gray-scale display threshold, the high-attenuation regions, i.e. the yellow and red areas are selected from the X-ray volume and neutron volume effectively identifying the densest inorganic or mineralized (Figure 2(c)) and main organic rich regions (Figure 2(d)), respectively. Figure 2(c) shows the pyrite pocket and the pyrite healed fracture that cuts through the layered structure at an oblique angle. Figure 2(d) highlights several areas with highly concentrated hydrogen content that corresponds to voids in the X-ray in addition to the overall dispersed organic content in the one half of the sample. It should be noted that even though the pocket and healed fracture in mineral-rich side of the rock highly attenuate neutron, they are not organic matter but are pyrite (see Figure 2(c)). The 3D structure of organic matter allows us to map the connection of kerogen 'globs' and fractures and, thus, suggests a possible flow path for light hydrocarbons at the core scale in this shale. Therefore, neutron tomography provides unique and significant information for modeling flow in shales in core scale.

Middle East shale. Figure 3 shows the simultaneous X-ray and neutron tomography slices for the Middle East shale. As described above, the regions outlined by solid green ovals are bright in the X-ray image but dark in the neutron image and, therefore, are occupied by minerals. There is a region outlined by short-dashed yellow oval that is bright in both X-ray and neutron images and is also mineral-rich. Based on the same reasons described for Barnett shale sample, these minerals may be anhydrite and pyrite for areas outlined by solid green ovals and short-dashed yellow oval, respectively. The regions outlined by solid red rectangles are dark on the X-ray image but bright in neutron image and likely are organic matter. There is a stripe which is dark in both neutron and X-ray images and is identified as fracture (outlined by long-dashed magenta rectangles).

Figure 4(a) and 4(b) are the 3D reconstructed images of the Middle East shale for X-ray and neutron modes, respectively. The colored regions are highly attenuated areas. By only displaying the high-attenuation regions, the distributions of inorganic and organic regions are plotted in Figure 4(c) and 4(d), respectively. Surprisingly, the organic matter has a clear layered structure with two layers at the top and in the center of the sample. This is very different from the structure of the organic matter found in the Barnett shale. Moreover, the inorganics are also clearly layered and form a continuous inorganic-rich layered shale (a.k.a. mud rock) (Figure 4(c)) and organic (Figure 4(d)) layers in the top and center of the sample.

The layered structures of organic matter have two important implications: first, it may give rise to fast path for light hydrocarbon movement. Second, it produces strong contrasts in mechanical properties which in turn may be weak surfaces along which the sample may break. The layer at the top of the sample, for example, is a broken face during plugging.

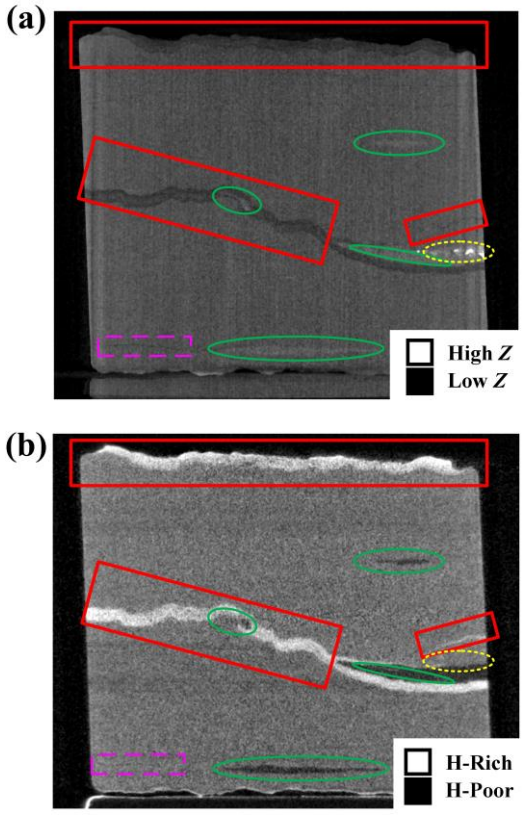

Fig. 3 Central slices of (a) X-ray and (b) neutron reconstructed volumes of the Middle East shale sample. The short-dashed yellow ovals and solid green ovals outline the mineral components of pyrite and probable anhydrite, respectively. Solid red rectangles outline the organic-rich regions

likely to be kerogens; the long-dashed magenta rectangles outline the fractures.

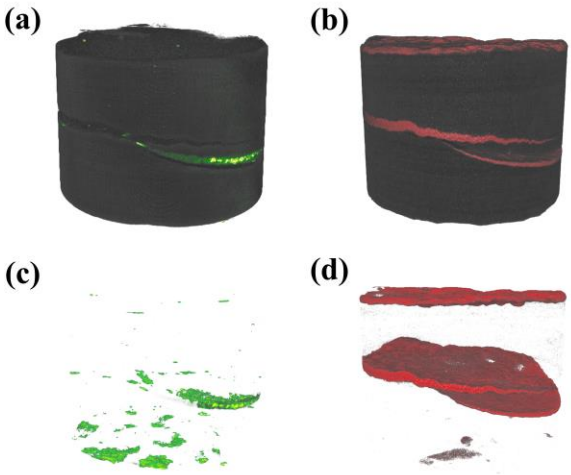

Fig. 4 3D volume renderings of the Middle East shale sample for (a) X-ray and (b) neutron tomography. Distributions of (c) high-Z components, i.e. the minerals, and (d) hydrogen-rich components, likely to be kerogens, are identified from the highly attenuated (colorized) regions in 3D X-ray and neutron tomography reconstructions, respectively.

DISCUSSIONS

The distributions of different components within shales are crucial for storage and transportation of hydrocarbons in the shales. The detailed structural description on the core scale of two shale samples demonstrates that simultaneous X-ray and neutron tomography is a powerful tool to quantify the distributions of organic and inorganic matter. With more information provided by the combined X-ray and neutron tomography, different minerals such as pyrite, calcite, and anhydrite can be distinguished. Moreover, since the hydrogen-rich organic matter and fractures are both very transparent to X-rays, it is challenging for the commonly used X-ray CT alone to unambiguously determine the organic matter distributions at the core scale. In contrast, neutrons are very sensitive to hydrogens and are useful to characterize the organic-rich shales. By combining X-ray and neutron tomography, more comprehensive information of material composition and distributions in shales are obtained.

It is worth mentioning that the component distributions found in this study are at the core scale, rather than the nanometer to micrometer pore scale. Current simulation and modeling of hydrocarbons are mostly based on the rock structure in pore scale constructed from SEM images (Chen et al. 2015; Jiang et al. 2017; Saraji and Piri 2015; Shabro et al. 2013). There is about a 10^9 order of magnitude upscaling in length scale from the pore to core scale. It will be a significant impact to study the influence of the distributions of different components within the rocks by simulating and modeling the hydrocarbon flow on core scale.

Since the wettability and surface properties are very different for the minerals and organic matter (Saraji et al. 2017), the structure and arrangement in space of these components can directly affect the storage and transportation of the hydrocarbons within the shale rocks (Chiang et al. 2016a; Chiang et al. 2016b). The two shale samples from two different formations exhibit very different organic matter structures. The laminar organic matter (kerogens) in the Middle East shale can dramatically change the current views of hydrocarbon flow and the mechanical properties in the shales.

CONCLUSIONS

The simultaneous X-ray and neutron tomography is necessary to more accurately characterize the distributions of different components such as minerals, organic matter, and fractures in the heterogeneous materials. In this study, the 3D characterizations of minerals and organic matter at the core scale are successfully demonstrated for the first time in shale samples from different locations. These results can be used in future simulation and modeling of hydrocarbon flow in core scale. In particular, the layered organic structure found in one of the shale samples can significantly change the current explanations of hydrocarbon flow in the shales.

ACKNOWLEDGEMENTS

The authors would like to thank Aramco for allowing the publication of this work. The technical work has benefited from discussions with colleagues at Aramco Research Center-Houston: Younane Abousleiman, Hui-Hai Liu.

REFERENCES

Aloulou, F., Zaretskaya, V.: Shale gas production drives world natural gas production growth - Today in Energy - U.S. Energy Information Administration (EIA), https://www.eia.gov/todayinenergy/detail.php?id=27512.

Ambrose, R.J., Hartman, R.C., Diaz Campos, M., Akkutlu, I.Y., Sondergeld, C.: New Pore-scale Considerations for Shale Gas in Place Calculations. In: SPE Unconventional Gas Conference. Society of Petroleum Engineers (2013).

Banhart, J., Borbély, A., Dzieciol, K., Garcia-Moreno, F., Manke, I., Kardjilov, N., Kaysser-Pyzalla, A.R., Strobl, M., Treimer, W.: X-ray and neutron imaging – Complementary techniques for materials science and engineering. Int. J. Mater. Res. 101, 1069–1079 (2010).

Chen, L., Zhang, L., Kang, Q., Viswanathan, H.S., Yao, J., Tao, W.: Nanoscale simulation of shale transport properties using the lattice Boltzmann method: permeability and diffusivity. Sci. Rep. 5, 8089 (2015).

Chiang, W.-S., Fratini, E., Baglioni, P., Chen, J.-H., Liu, Y.: Pore Size Effect on Methane Adsorption in Mesoporous Silica Materials Studied by Small-Angle Neutron Scattering. Langmuir. 32, 8849–8857 (2016)(a).

Chiang, W.-S., Fratini, E., Baglioni, P., Georgi, D., Chen, J., Liu, Y.: Methane Adsorption in Model Mesoporous Material, SBA-15, Studied by Small-Angle Neutron Scattering. J. Phys. Chem. C. 120, 4354–4363 (2016)(b).

Jiang, W., Lin, M., Yi, Z., Li, H., Wu, S.: Parameter Determination Using 3D FIB-SEM Images for Development of Effective Model of Shale Gas Flow in Nanoscale Pore Clusters. Transp. Porous Media. 117, 5–25 (2017).

Kienzle, P.: Neutron Activation Calculator, https://www.ncnr.nist.gov/resources/activation/.

LaManna, J.M., Hussey, D.S., Baltic, E., Jacobson, D.L.: Neutron and X-ray Tomography (NeXT) system for simultaneous, dual modality tomography. Submitted to Review of Scientific Instruments (2017).

Limaye, A.: Drishti: a volume exploration and presentation tool. In: Stock, S.R. (ed.) Developments in X-Ray Tomography VIII. p. 85060X. International Society for Optics and Photonics (2012).

Loucks, R.G., Reed, R.M., Ruppel, S.C., Jarvie, D.M.: Morphology, Genesis, and Distribution of Nanometer-Scale Pores in Siliceous Mudstones of the Mississippian Barnett Shale. J. Sediment. Res. 79, 848–861 (2009).

Manke, I., Banhart, J., Haibel, A., Rack, A., Zabler, S., Kardjilov, N., Hilger, A., Melzer, A., Riesemeier, H.: *In situ* investigation of the discharge of alkaline Zn–MnO2 batteries with synchrotron x-ray and neutron tomographies. Appl. Phys. Lett. 90, 214102 (2007)(a).

Manke, I., Hartnig, C., Grünerbel, M., Lehnert, W., Kardjilov, N., Haibel, A., Hilger, A., Banhart, J., Riesemeier, H.: Investigation of water evolution and transport in fuel cells with high resolution synchrotron x-ray radiography. Appl. Phys. Lett. 90, 174105 (2007)(b).

Mannes, D., Benoît, C., Heinzelmann, D., Lehmann, E.: Beyond the Visible: Combined Neutron and X-ray Imaging of an Altar Stone from the Former Augustinian Church in Fribourg, Switzerland. Archaeometry. 56, 717–727 (2014).

Mannes, D., Schmid, F., Frey, J., Schmidt-Ott, K., Lehmann, E.: Combined Neutron and X-ray Imaging for Non-invasive Investigations of Cultural Heritage Objects. Phys. Procedia. 69, 653–660 (2015).

Saraji, S., Piri, M.: The representative sample size in shale oil rocks and nano-scale characterization of transport properties. Int. J. Coal Geol. 146, 42–54 (2015).

Saraji, S., Piri, M., Akbarabadi, M., Georgi, D., Delshad, M.: Nano-scale Experimental Investigation of In-situ Wettability and Spontaneous Imbibition in Ultra-tight Reservoir Rocks. Submitted to Water Resources Research (2017).

Seltzer, S.M.: NIST X-Ray Form Factor, Atten. Scatt. Tables Form Page, http://physics.nist.gov/PhysRefData/FFast/html/form.html.

Shabro, V., Kelly, S., Torres-Verdín, C., Sepehrnoori, K.: Pore-Scale Modeling of Electrical Resistivity and Permeability in FIB-SEM Images of Hydrocarbon-

Q

Bearing Shale. In: SPWLA 54th Annual Logging Symposium, 22-26 June, New Orleans, Louisiana. Society of Petrophysicists and Well-Log Analysts (2013).

Siskin, M., Scouten, C.G., Rose, K.D., Aczel, T., Colgrove, S.G., Pabst, R.E.: Detailed Structural Characterization of the Organic Material in Rundle Ramsay Crossing and Green River Oil Shales. In: Composition, Geochemistry and Conversion of Oil Shales. pp. 143–158. Springer Netherlands, Dordrecht (1995).

Zhang, T., Yang, R., Milliken, K.L., Ruppel, S.C., Pottorf, R.J., Sun, X.: Chemical and isotopic composition of gases released by crush methods from organic rich mudrocks. Org. Geochem. 73, 16–28 (2014).

APPENDIX

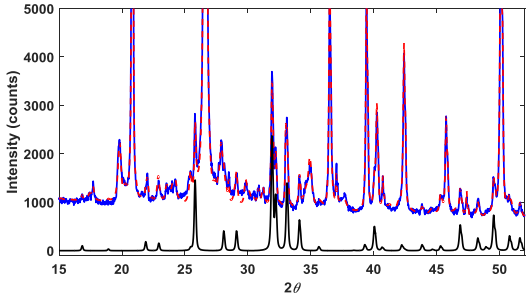

Fig. A1 XRD of the Barnett shale sample. The blue spectrum is the diffractogram from a Bruker D8 Advance Eco (at 40kV 25 mA with a 0.6mm divergent slit; two 2.5° soller slits; and a LynxEye Detector with all 192 channels used). The red trace is the simulated pattern using Bruker's Topas with the reported minerals; the black trace shows the simulated pattern for the mineral Fluorapatite. The amounts of the minerals are validated using another Rietveld software Autoquan/BGMN.

Q